Journal of Power Sources 195 (2010) 3590–3596

Contents lists available at ScienceDirect

Journal of Power Sources

journal homepage: www.elsevier.com/locate/jpowsour

Localised corrosion processes of austenitic stainless steel bipolar plates for polymer electrolyte membrane fuel cells

Claudio Mele*, Benedetto Bozzini

Dipartimento di Ingegneria dell'Innovazione, Università del Salento, via Monteroni, 73100 Lecce, Italy

ARTICLE INFO

Article history:
Received 31 August 2009
Received in revised form
24 November 2009
Accepted 27 November 2009
Available online 16 December 2009

Keywords:
PEMFC
Bipolar plates
Stainless steel
Localised corrosion
Crevice

ABSTRACT

This research addresses the problem of localised corrosion of stainless steel PEMFC bipolar plates. The susceptibility to pitting and crevice corrosion of austenitic AISI 304 stainless steel has been investigated both by post-mortem microscopic analysis of the end-plates of a laboratory single-cell and by studies of electrochemically corroded stainless steels, in the presence of specially-designed crevice-formers simulating the operating conditions of a PEMFC. This work is based on optical and scanning-electron microscopies as well as potentiostatic and potentiodynamic measurements. The crevice-formers we considered were: Teflon, graphite and AISI 304. The samples, coupled to the crevice-formers have been tested in aqueous solutions containing Cl^-, SO_4^{2-} and F^-. From the E–log i plot, the values of corrosion, pitting, crevice and protection potential have been obtained and perfect and imperfect passivity conditions have been identified.

© 2009 Elsevier B.V. All rights reserved.

1. Introduction

Bipolar plates (BPs) are a key component of PEM hydrogen fuel cell (FC) stacks, from both functional and structural points of view. BPs conduct electric current across the stack, contain the conduits for reactant gases and contribute to water and heat balances. Graphite and graphite-based composites can be regarded as the standard materials implemented in BP fabrication. Nevertheless, this class of materials, notwithstanding their low surface electrical resistance and relatively high corrosion resistance, is far from optimal, essentially owing to: brittleness, permeability to reactant gases and relatively low cost-effectiveness, in the prospective scenario of automated mass-production. In this respect, metals are currently considered an attractive alternative, especially for transportation applications, and many studies have started to appear in the literature, proposing different concepts of metal-based BPs: an updated list is reported in [1]. Briefly, the appeal of metallic BPs lies in the following aspects: (i) higher mechanical strength and toughness with respect to graphite; (ii) no appreciable permeability to gases; (iii) ease of forming and fabrication. A useful list of target requirements for metallic BPs is reported in the outstanding, recent review [2]. As far as drawbacks are concerned, corrosion resistance is the chief one, in that the acidic aqueous environment of the PEMFCs gives rise to: (i) formation of passive layers with attending increment of the electrical contact resistance; (ii) release of ions that can further react with FC materials, potentially leading to the clogging of the porous components (GDEs and ion-exchange membranes) and poisoning of the catalysts (e.g. [3]); (iii) formation of perforating pinholes through the plates.

In addition to suitably-formed metal sheet, metallic foams have also been proposed for the fabrication of BPs, in order to achieve gas flow directly in the pores, as an alternative to the traditional channel-flow design [4]; the materials investigated were: AISI 316 stainless steel and Fe8,Cr30–54,C2,Ni(balance). Furthermore, bipolar materials using CNT/PTFE nanocomposites have been proposed as coatings for stainless steel, in order to achieve higher durability and reduction in contact resistance between BP and gas-diffusion layer (GDL) [5].

The test environments used in published BP corrosion studies are summarised in [1]. As far as the investigation methods are concerned, the following approaches have been reported in the literature: (i) open circuit potential measurements [6–14], (ii) potentiostatic polarisation [6–9,12–29], (iii) polarisation resistance [26,30,31], (iv) linear-sweep voltammetry [6,32,33], (v) I–V and I–P curves as well as a limited number of life time tests in fuel cell assemblies [23,34–36]. A few instances of compositional measurements on films formed on stainless steel have also been reported, based on XPS [18,29] and EDS [2,27,28]. Further characterisation of the surface resistivity of BP materials is sometimes carried out by resistance measurements under known compaction forces, typically in the range 100–300 N cm^{-2} [2,7,8,11,12,23,26–29,37].

* Corresponding author. Tel.: +39 0832 297621; fax: +39 0832 297621.
E-mail address: claudio.mele@unisalento.it (C. Mele).

0378-7753/$ – see front matter © 2009 Elsevier B.V. All rights reserved.
doi:10.1016/j.jpowsour.2009.11.144

Localised corrosion in BPs based on stainless steel has received limited attention, so far. Nevertheless, it seems to be an important damage mechanism, able to impair gas flow through the generation of defects in the channels, that have been proved to have a remarkable bearing on condensed water flow and flooding [38] as well as on hydraulic tightness, giving rise to the release of obnoxious cations.

The aim of this work is to highlight localised corrosion problems for BPs, with special attention to crevice corrosion of austenitic AISI 304 stainless steel, a classical candidate material for the relevant application. In the first part of the paper, localised corrosion has been highlighted in metallic plates after prolonged operation of a laboratory single-cell PEMFC. In the second part of this study, several tests were performed without and with crevice-formers. In this way, on the basis of literature data-analysis methods [39,40], two kinds of localised corrosion potential can be defined: a pitting (E_{pit}) and a crevice potential (E_{crev}), found in the absence and in the presence of a crevice-former, respectively. Moreover, the choice of metallic and non metallic crevice-formers was made, in order to pinpoint the special type of corrosion system relevant to our case, where the crevice-former (GDL) also acts as the nobler element of a galvanic couple. In order to simulate an environment typical of the prolonged operation of a PEMFC, we employed solutions containing Cl^-, SO_4^{2-} and F^- ions. The presence of SO_4^{2-} and F^- ions in the electrolyte of a fuel cell is mainly due to the degradation of Nafion [41], the presence of Cl^- ions is related to pollution of reactant gas, oxygen and hydrogen – especially in important, power-intensive applications like submarines – potentially occurring along every section of the gas-handling system, or to the degradation of MEA, giving rise to the release of Cl^- as a result of the use of chlorine in the production process [42].

2. Experimental

In the first part of this research, we concentrated on the anodic and cathodic BPs of a single-cell laboratory PEMFC, purchased from Materials Mates Italia. The cell included two square (5 cm × 5 cm) BPs – depicted in the macrographs reported in Fig. 1 in the typical pristine condition – fabricated by punching AISI 304 foils of thickness 200 μm. The GDLs were carbon paper and the C-supported Pt catalyst was applied to the Nafion membrane. The cell was operated for a 1000 h run. Gas was fed to the cell through a gas-control manifold, connected to compressed-gas bottles. The cathode was fed with compressed air at room temperature and a flow rate of 2 LPM. The anode was fed with a mixture of N_2 and H_2, humidified at 40 °C. The N_2 and H_2 flow rates were adjusted during the run, as detailed below, in order to keep the working point of the PEMFC as constant as possible, of course within the limits of a very basic laboratory system. Electrical control of the FC was performed with an AMEL 7050 potentiostat, setting potentiostatic conditions at 0.6 V. The initial and final (i.e. after 1000 h of operation) OCP values (recorded for 1 h at the current gas feed conditions) were: 948 ± 0.9 and 965 ± 1.0 mV, respectively. The current extracted (±1 standard deviation) at 0.6 V was 628 ± 23 mA. The anodic gas flow rates were adjusted in the following ways: (i) 0–115 h: H_2 0.2 LPM, N_2 1.0 LPM; (ii) 115–510 h: H_2 0.2 LPM, N_2 0.75 LPM; (iii) 510–805 h: H_2 0.5 LPM, N_2 0.75 LPM; (iv) 805–895 h: H_2 0.5 LPM, N_2 1.0 LPM to contrast flooding; (v) 895–960 h: H_2 0.5 LPM, N_2 1.25 LPM same reason; (vi) 960–1000 h: H_2 1.0 LPM, N_2 1. 5 LPM to try and counteract overall cell performance degradation. Optical macro- and micrographs and SEM images of the investigated anodic and cathodic BPs have been obtained using a Nikon Epiphot 200 OM and a Cambridge Stereoscan 360 SEM, respectively.

In order to gain more detailed information about the localised effects of galvanic coupling and of geometrical screening deriving from the mechanical junction between carbonaceous materials and

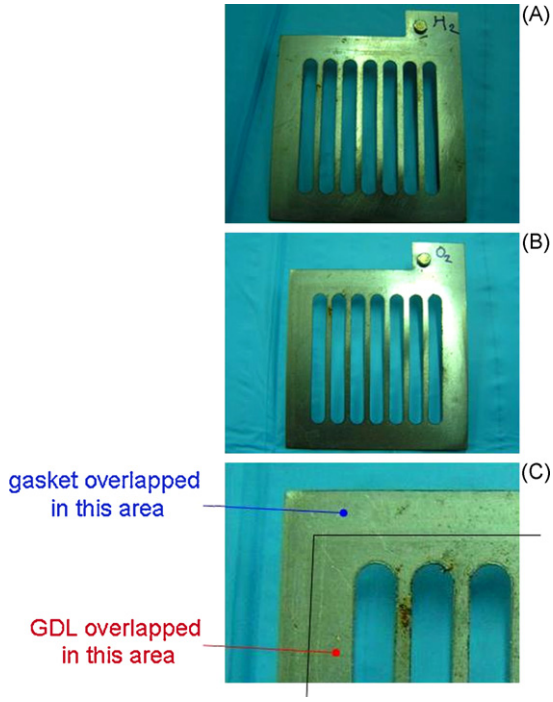

Fig. 1. Macrographs of the BPs (5 cm × 5 cm) after 1000 h of operation in a PEMFC. Side facing the GDL: (A) anodic BP, (B) cathodic BP, and (C) detail of the cathodic BP, showing the location of the rubber gasket and C-paper GDL.

stainless steel, we studied the effects of contacting slabs of AISI 304 and blocks of reticulated vitreous carbon (RVC) (see, e.g. [43] and references therein contained). We pressed four 3 cm × 2 cm stainless steel slabs against samples of RVC (Electrosynthesis–Lancaster NY, mesh 100 PPI: the samples we used are a gratefully acknowledged present of Dr. Sheelagh Campbell's–Portsmouth University) of the same dimensions, with a nominal pressure of 10 N and plunged the system in an aerated 0.5 M H_2SO_4 solution. We carried out two types of experiments: (i) immersion tests and (ii) electrochemical tests (potentiostatic and potentiodynamic).

Finally, in order to investigate crevice corrosion by electrochemical methods, the samples of AISI 304 austenitic stainless steel (plate of 20 mm × 40 mm, thickness 1 mm) were fitted with a crevice-former. It is worth recalling here that – according to [44] – we define "crevice corrosion" as the "localised corrosion of a metal surface at, or immediately adjacent to, an area that is shielded from full exposure to the environment because of close proximity between the metal and the surface of another material". In this sense, within the realm of BP corrosion, by using the term "crevice" we refer to the special localised corrosion effects deriving from the fact that different materials, exhibiting different properties in terms of electrical conductivity, are mechanically coupled to the metallic BP. In order to obtain reproducible results, prior to the measurements, each specimen was pre-treated according to the procedure recommended in [45], consisting in: mechanical polishing with emery papers of different grades down to 2400 grit, degreasing with acetone, rinsing with bi-distilled water. The sample was covered with epoxy resin on the back side and immersed in the bath leaving a controlled exposed surface area of 20 mm × 20 mm. A Teflon, graphite or AISI 304 stainless steel rectangular crevice-former of area 20 mm × 10 mm – designed to simulate the geometry of the coupling between bipolar plate and gas-diffusion layer characterised by the sequence rib-channel – was fixed onto the front face of the sample and compressed uniformly with a force of 100 ± 10 N. This value was estimated using a home-made instrumented laboratory press, specially designed for fuel cell applications. Experiments

were carried out at room temperature in a 10 mM H_2SO_4 solution, prepared with ultrapure water with a resistivity of 18 MΩ from a Millipure Milli-Q system. To this solution, 10 mM HCl and/or 15 ppm HF were added. During the test, air was bubbled continuously to simulate the cathode environment. Electrochemical measurements were conducted in a three-electrode cell using an AMEL 5000 programmable potentiostat/galvanostat. A platinised Ti expanded-mesh sheet with a surface area of 30 cm^2 and a Ag/AgCl electrode were used as counter (CE) and reference electrodes (RE), respectively. The RE was connected to a Luggin capillary filled with the test electrolyte. The tip of the Luggin capillary was located at ca. 1 mm from the WE. All potentials are reported against Ag/AgCl. At the beginning of each experiment, the WE was cathodically polarised at −700 mV for 5 min to remove surface oxide and to assure reproducibility [7]. Then, the samples, with or without crevice-former, were subjected to cyclic anodic potentiodynamic polarisation at a scan rate of 1 mV s^{-1}. Forward anodic polarisation was applied from −700 to 800 mV in a first series of experiments and from −700 to 1600 mV in a second one. The first anodic terminal potential corresponds to typical value suggested by ASTM crevice corrosion tests [46]. The second one has been chosen in order to discriminate the corrosion effects of different ions added to the electrolyte. More details are reported in Section 3.3. The anodic terminal potential was maintained for 1 h, monitoring the corresponding current density and then the reverse polarisation was performed up to the achievement of the repassivation conditions. From the E–log i plot, the values of corrosion (E_{corr}), pitting (E_{pit}), crevice (E_{crev}) and protection potential (E_{prot}) were obtained; from these quantities, perfect and imperfect passivity conditions were defined. E_{crev} or E_{pit} can be determined in correspondence of the increased current density recorded during the forward polarisation, and E_{prot} at the crossing between the reverse and the forward scan [47–51]. Each measurement was repeated thrice and the E_{corr}, E_{pit}, E_{crev}, E_{prot} values reported below correspond to the mean ± 1 standard deviation.

3. Results and discussion

3.1. Corrosion of stainless steel bipolar plates in a laboratory single-cell

In Fig. 1 we report the macrographs of whole anodic (A) and cathodic (B) BPs. Some rust spots can be noticed, as well as marks corresponding to the area where the metal contacts the rubber gasket and the C-paper GDL (see (C) for a magnification of the cathodic BP).

Optical micrographs of the anodic (A) and cathodic (B) BPs are shown in Fig. 2. The micrographs display a selection of attack morphologies, chosen from several locations of the sides of the BPs facing the GDL and are arranged in the form of pseudo-ribs, of course not to scale, just for graphical convenience. Images from a pristine BP are reproduced in Fig. 2A, for comparison. Several localised attack features show up in both the anodic and the cathodic BPs after 1000 h of operation. Severe attack seems to develop at the cathodic BP, that exhibits more extensive pitting and deeper damage penetrations at the rib side, in comparison with the anodic BP.

A more detailed investigation of the transition area of the cathodic and anodic BPs, mated to the rubber gasket and to the C-paper GDL (see Fig. 1C) has been performed by SEM, the results are depicted in Fig. 3. Both anodic and cathodic BPs exhibit a localised corrosion form at such interface, the severer attack corresponding to the zone under the gasket, showing a significantly narrower crevice with the stainless steel surface, owing to the higher compliance of rubber with respect to carbon paper.

3.2. Corrosion of stainless steel, mechanically coupled with reticulated vitreous carbon

3.2.1. Immersion tests

AISI 304 coupons have been coupled, as described in Section 2 with RVC samples and exposed to an acidic sulphate solution.

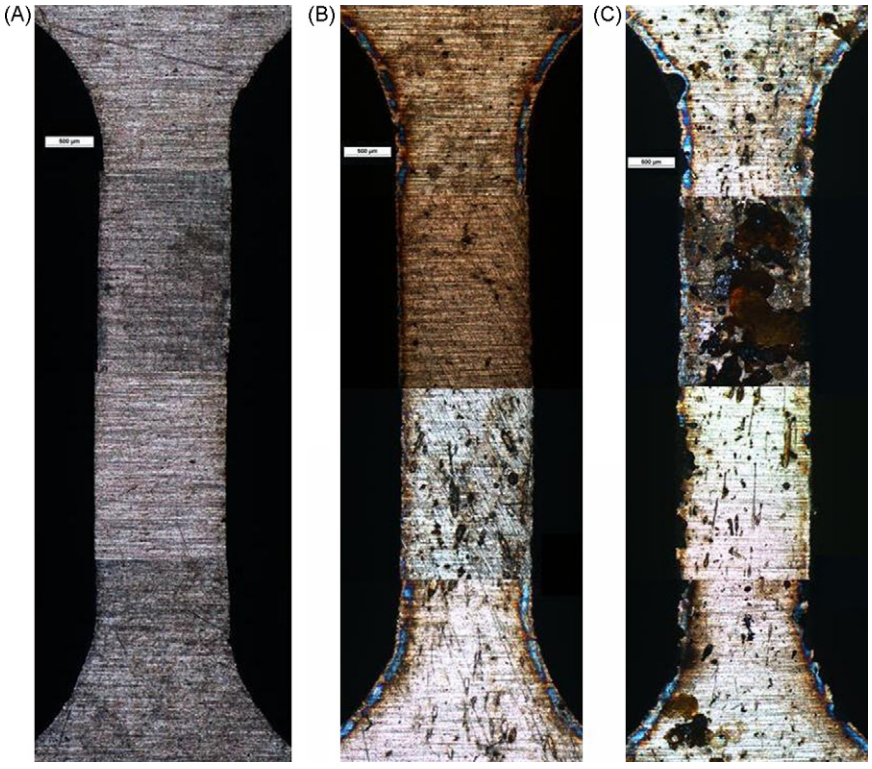

Fig. 2. Optical micrographs of several locations (assembled in the form of a pseudo-rib, for graphical convenience) of the BPs (5 cm × 5 cm) after 1000 h of operation in a PEMFC. Side facing the GDL: (A) pristine BP, (B) anodic BP, and (C) cathodic BP.

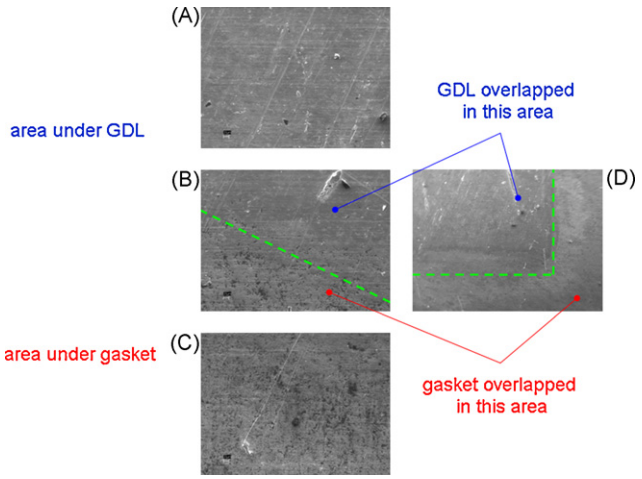

Fig. 3. SEM micrographs of the cathodic (A–C) and anodic (D) BPs after 1000 h of operation in a PEMFC. (B) and (D) show the cathodic and anodic areas, respectively, that are partially covered by the rubber gasket and by the C-paper GDL. (A) and (C) show regions of the cathodic BP in contact with the gasket and the GDL, respectively. All micrographs have the same magnification. The green, dashed lines indicate the position of the edge between the gasket and the GDL. (For interpretation of the references to color in this figure legend, the reader is referred to the web version of the article.)

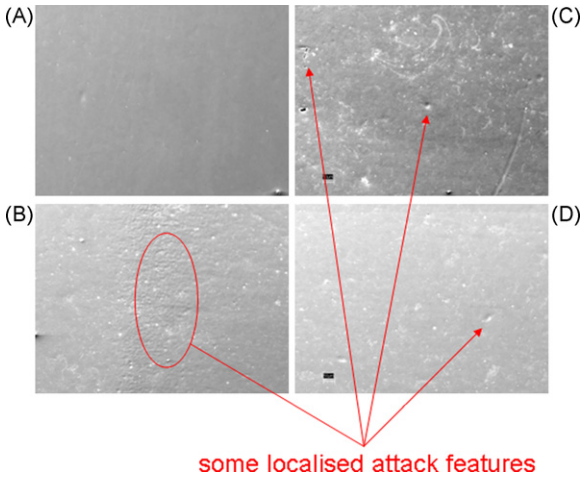

Fig. 4. SEM micrographs of AISI 304 (A) and AISI 304 coupled to RVC (B–D), after immersion in areated 0.5 M H_2SO_4 for 3 months. All micrographs have the same magnification. A selection of localised attack features, out of the many present, are highlighted.

For comparison, we also placed, close to the test assembly, but not in contact with it, a reference stainless steel slab. Five replicated systems were built. After a waiting time of 3 months, the assemblies were opened and examined by SEM. In Fig. 4, we reproduce a selection of typical micrographs, showing that a number of localised corrosion features develop at the contact points between the steel surface and the RVC, in the form of isolated or clustered pits, as highlighted on the image. In particular, micrograph (A) shows the typical morphology of an AISI 304 surface immersed in the aerated acidic solution without contact to the RVC: over a large area, no attack features can be noticed and the overall appearance is essentially smooth. To the contrary, micrographs (B–D), report a representative selection of attack morphologies found on AISI 304 surfaces coupled to the RVC. Such surfaces are generally rougher and exhibit localised corrosion features, that correspond to points or areas of contact between the mating materials, that can be interpreted as resulting from the combined action of galvanic coupling to the more noble carbonaceous material, alongside with geometrical shielding, leading to so-called crevice corrosion.

3.2.2. Electrochemical tests

Comparative electrochemical tests were run with AISI 304, RVC and AISI 304 coupled to RVC. The location of the reference electrode (tip of the Piontelli probe) is illustrated in Fig. 5. In Fig. 6 we show potentiodynamic measurements carried out at a scan rate of 1 mV s^{-1} with AISI 304 in the absence and in the presence of coupling to RVC. Coupling to RVC gives rise to higher c.d.s as well as to an ennobling of the corrosion potential, both before and after potentiodynamic polarisation. It is worth noting that the passivation peak cannot be noticed with the galvanically mated sample. The effect of coupling the RVC to AISI 304 on the OCP of a pristine stainless steel sample can be observed in the inset of Fig. 6. Since RVC exhibits a wide electrochemical window in the relevant electrolyte (see also Fig. 7), the additional c.d. resulting from coupling can be entirely attributed to the stainless steel.

In Fig. 7 we report potentiostatic measurements carried out at 1.2 V vs. Ag/AgCl for RVC, AISI 304 and AISI 304 coupled to RVC. These data confirm the results of Fig. 6, showing that a higher anodic c.d. is established when AISI 304 is coupled to RVC and that RVC alone bears a vanishing c.d. under the relevant electrochemical conditions (Fig. 7A).

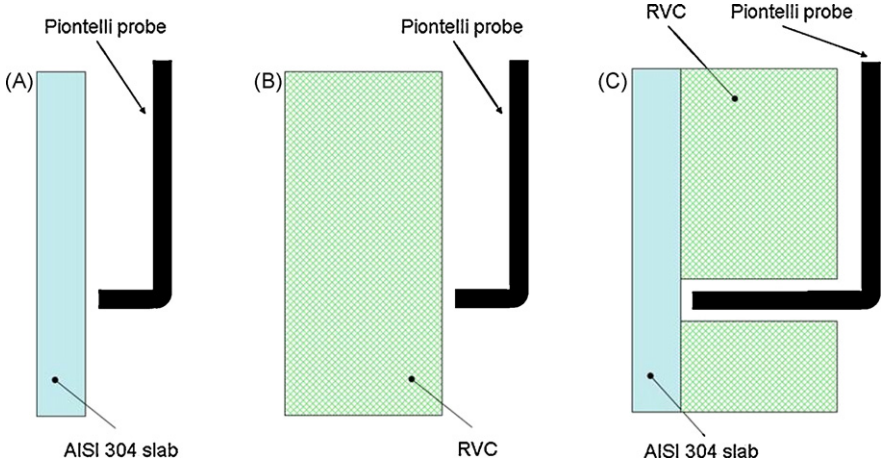

Fig. 5. Collocation of the reference–electrode connection via Piontelli probe in the electrochemical experiments carried out with different combinations of AISI 304 and RVC electrodes.

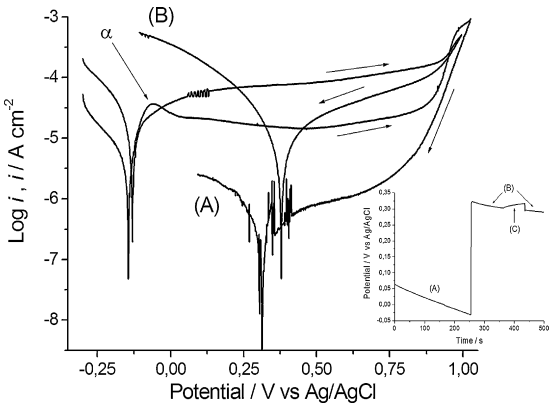

Fig. 6. Potentiodynamic curves of AISI 304 (A) and AISI 304 coupled to RVC (B). Scan rate: 1 mV s^{-1}, scan direction indicated on the plot. Inset: OCP for (A) AISI 304, (B) AISI 304 coupled to RVC, (C) RVC.

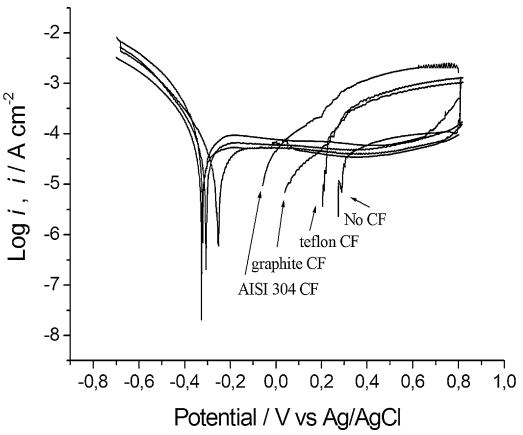

Fig. 8. Anodic polarisation curves recorded using AISI 304 samples without and with crevice-formers in a solution containing 10^{-3} M H_2SO_4 and 10^{-2} M HCl.

3.3. Electrochemical measurements in the presence of crevice-formers

The propensity of stainless steel grades towards localised corrosion in a given environment may be assessed in a relatively short-time using potentiodynamic polarisation tests, even if the values of E_{pit} (or E_{crev}) and E_{prot} obviously depend on the scan rate used and on the geometry of the crevice-former [47,52,53]. In Fig. 8 we report a series of potentiodynamic polarisation cycles, carried out with Teflon, graphite and AIS 304 crevice-formers. These electrochemical measurements were carried out with the anodic terminal potential set to 800 mV; this value has been chosen because it is both close to a typical operation voltage of a PEMFC [19,20,22] and it corresponds to conditions suggested by ASTM crevice corrosion tests [46]. The plotted curves correspond to experiments carried out without and with crevice-formers in the solution containing H_2SO_4 and HCl. During the potential scan in the anodic direction, for potentials positive of the free-corrosion value, an anodic current density plateau appears, ascribed to the formation of passive film, followed by a transpassive region with a drastic increase in the anodic current density, probably due to the oxidation of trivalent chromium to the exavalent state [29]. The curves show a well-defined hysteresis loop whence the determination of characteristic potentials is straightforward. E_{corr}, E_{crev} (or E_{pit}) and E_{prot} values obtained from this curves are reported in Fig. 9. The curve corresponding to the uncreviced specimen, shows a narrow hysteresis loop, indicating a rapid achievement of repassivation conditions. A narrow hysteresis is, in general, indicative of a low susceptibility of a metal to the localised attack in a given environment [53]. The E_{corr} values of the crevice couples were close to that of the uncreviced AISI 304, in the case of Teflon and graphite crevice-formers, suggesting that the corrosion potential is dominated by the behaviour of stainless steel . In the case of the graphite crevice-former, the E_{corr} value was less cathodic: this is consistent with reported galvanic series in flowing sea water [54]. The estimated E_{corr}, E_{crev} (or E_{pit}) and E_{prot} values can be used to define two regions in the E–log i plot for a material in a given environment: (i) the perfect passivity region (*ppr*) corresponding to potentials less positive than E_{prot}, where the pitting corrosion cannot initiate and pre-existing pits cannot propagate and (ii) the imperfect

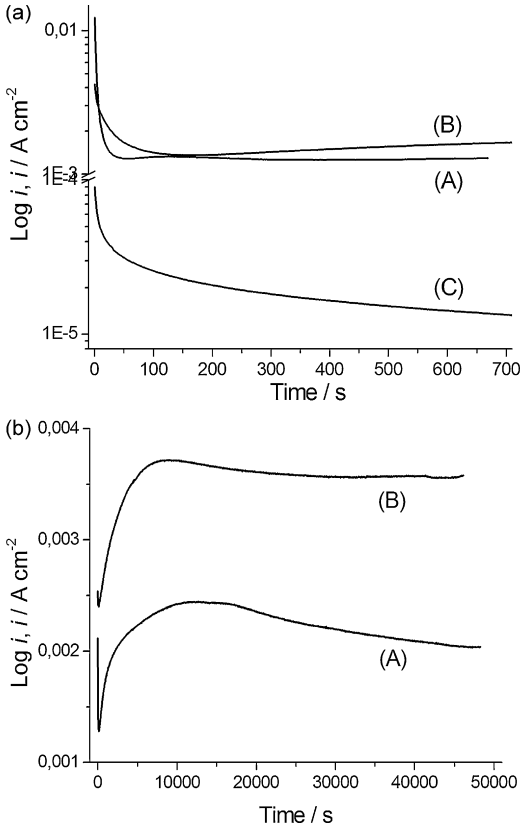

Fig. 7. Potentiostatic measurements at 1.2 V vs. Ag/AgCl of: (A) AISI 304, (B) AISI 304 coupled to RVC, (C) RVC. Panel (a) short-time measurements and comparison with RVC; panel (b) long-time measurement.

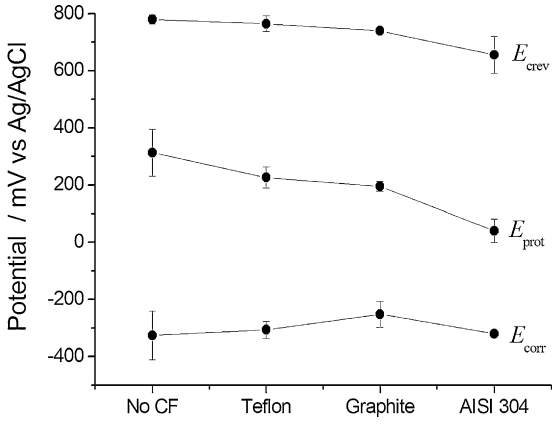

Fig. 9. E_{corr}, E_{crev} (or E_{pit}) and E_{prot} values obtained from the polarisation curves of Fig. 8, using AISI 304 samples without and with crevice-formers in a solution containing 1 mM H_2SO_4 and 10 mM HCl.

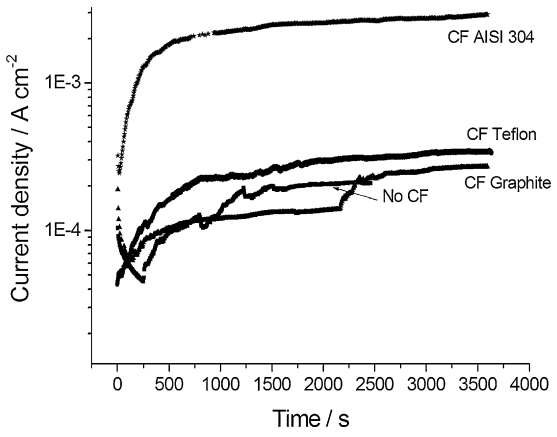

Fig. 10. Potentiostatic plots obtained at 800 mV, at the end of the forward anodic polarisation, using AISI 304 samples without and with crevice-formers in a solution containing 1 mM H_2SO_4 and 10 mM HCl.

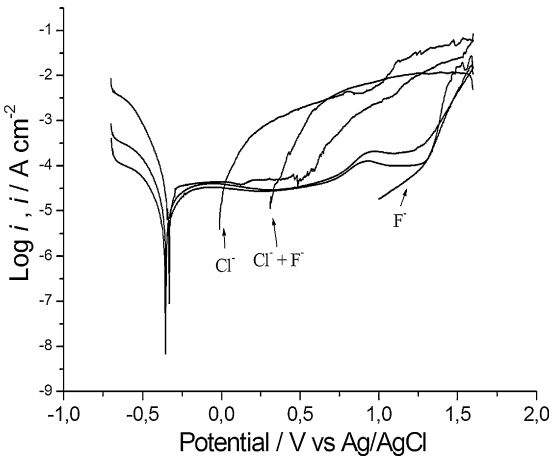

Fig. 11. Anodic polarisation curves recorded using AISI 304 samples with a graphite crevice-former in the solution containing 1 mM H_2SO_4 and (a) 15 ppm HF, (b) 10 mM HCl, (c) 10 mM HCl + 15 ppm HF.

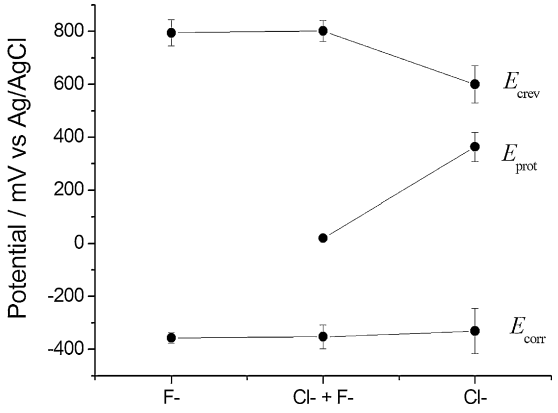

Fig. 12. E_{corr}, E_{crev} (or E_{pit}) and E_{prot} values obtained from the polarisation curves plotted in Fig. 11, using AISI 304 samples without and with crevice-formers in a solution containing 1 mM H_2SO_4 and (a) 15 ppm HF, (b) 10 mM HCl, (c) 10 mM HCl + 15 ppm HF.

passivity region (*ipr*), defined by the potential range between E_{pit} and E_{prot}, where pits cannot initiate, but existing pits can propagate [45,55,56]. E_{corr} has been used as the lower limit of *ppr* in order to obtain a graphic delimitation of *ppr*, useful to visualize the region where the material remains passive and is preserved from localised corrosion [56]. From Figs. 8 and 9, one can conclude that, after localised corrosion is started, the stainless steel AISI 304 in the investigated electrolyte does not show a marked tendency to repassivate, as indicated by the high amplitude of the imperfect passivity region. In particular, E_{crev}, in the presence of Teflon or graphite crevice-formers, is slightly lower than E_{pit} measured with the uncreviced specimen, whereas the stainless steel AISI 304 crevice-former gives rise to a more serious attack condition, witnessed my the much wider loop, visible in Fig. 8.

Fig. 10 shows the current density measured by applying a constant potential of 800 mV at the end of the forward anodic scan. In all cases, the current density increases with time, reaching an asymptotic value. In particular, with the stainless steel crevice-former, the asymptotic current density is one order of magnitude higher with respect to the other cases, as expected from the literature concerning the mating of two stainless steel surfaces [54]. In the case of Teflon or graphite crevice-former, the increase in the current density was instead limited, as well as the width of the corresponding loop observed in the reverse scan. In the case of an uncreviced specimen, the increase in current and the current loop width were, of course, smaller. These observations suggest that this particular stainless steel grade is susceptible to crevice corrosion under the relevant conditions, but its susceptibility is not highly affected by the use of Teflon (electrically insulating) or graphite (electronically conducting, but not able to release corrosion products) crevice-forming, whereas an AISI 304 crevice-former (corroding and releasing hydrolysing Fe-group metal ions in the crevice) exhibits a major effect.

In order to better discriminate the effects of different ions added to the electrolyte, simulating FC operating conditions, we resorted to an approach able to amplify the current density loop related to crevice corrosion in the reverse potentiodynamic scan, by shifting the anodic terminal voltage well into the transpassive region [57]. The curves obtained by using a graphite crevice-former and an anodic terminal potential of 1600 mV have been plotted in Fig. 11. The E_{corr}, E_{crev} (or E_{pit}) and E_{prot} values, estimated from the curves of Fig. 11, are reported in Fig. 12. The largest loop, corresponding to a less anodic value of E_{prot}, can be observed in the case of solution containing only SO_4^{2-} and Cl^- ions. With the SO_4^{2-} and F^- ions, the loop is hardly visible, instead. An intermediate result is obtained with solutions simultaneously containing all the investigated ions: SO_4^{2-}, Cl^- and F^-. As expected, Cl^- ions are found to be the most aggressive in terms of crevice corrosion, whereas the effect of the F^- is negligible in the absence of Cl^- and exhibits an inhibiting action in its presence, yielding narrower current density loops and more anodic E_{prot} values. As far as ion effects are concerned, the same ranking was found to apply both in the absence and in the presence of a crevice-former, regardless of the material it consists of.

4. Conclusions

During 1000 h of operation of a laboratory single-cell PEMFC, both anodic and cathodic AISI 304 BPs have been found to exhibit localised corrosion effects at the interface with the rubber gasket and the C-paper GDL, apparently due to material coupling and type of gas feed. Severe attack seems to develop at the cathodic BP. In addition to highlighting such localised corrosion effects, in this paper we propose a first approach to their rationalisation in terms of electrochemical experiments with different types of crevice-formers and ion contaminations. This method is expected to provide a useful tool for the simulation of material stability for BPs under PEMFC operating conditions. In particular, we tested the peculiar localised corrosion effects, that can be described as crevice corrosion, resulting from the coupling AISI 304 to the carbon GDL; for comparison we also tested Teflon and AISI 304 crevice-formers.

Such electrochemical testing has been quantified in terms of perfect and imperfect passivity conditions. In particular, E_{crev} in the presence of Teflon or graphite crevice-formers results to be slightly lower than E_{pit} measured with the uncreviced specimen, whereas the AISI 304 crevice-former gives rise to enhanced localised attack. The impact of typical ionic contaminants (Cl^- and F^-) on crevice corrosion has been investigated, too. Cl^- ions are more aggressive, the effect of F^- in the absence of Cl^- is negligible, whereas F^- ions added to a solution containing Cl^- act as an inhibitor both in the absence and in the presence of any of the investigated types of crevice-former.

Acknowledgments

Expert assistance with electrochemical experiments of Mr. Francesco Bogani and Mr. Pierandrea Tafuro is gratefully acknowledged.

References

[1] B. Bozzini, I. Sgura, SIAM J. Appl. Math. 70 (2009) 579–599.
[2] H. Tawfik, Y. Hung, D. Mahajan, J. Power Sources 163 (2007) 755–767.
[3] V. Mehta, J.S. Cooper, J. Power Sources 144 (2003) 32–53.
[4] A. Kumar, R.G. Reddy, J. Power Sources 129 (2004) 62–67.
[5] Y. Show, K. Takahashi, J. Power Sources 190 (2009) 322–325.
[6] Y. Wang, D.O. Northwood, Electrochim. Acta 52 (2007) 6793–6798.
[7] R.F. Silva, D. Franchi, A. Leone, L. Piloni, A. Masci, A. Pozio, Electrochim. Acta 51 (2006) 3592–3598.
[8] R.J. Tian, J.C. Sun, L. Wang, Int. J. Hydrogen Energy 31 (2006) 1874–1878.
[9] H. Iken, R. Basseguy, A. Guenbour, A.B. Bachir, Electrochim. Acta 52 (2007) 2580–2587.
[10] A.M. Lafront, E. Ghali, A.T. Morales, Electrochim. Acta 52 (2007) 5076–5085.
[11] A. Pozio, F. Zaza, A. Masci, R.F. Silva, Int. J. Power Sources 179 (2008) 631–639.
[12] Y. Fu, M. Hou, H. Xu, Z. Hou, P. Ming, Z. Shao, B. Yi, J. Power Sources 182 (2008) 580–584.
[13] A. Pozio, R.F. Silva, A. Masci, Int. J. Hydrogen Energy 33 (2008) 5697–5702.
[14] H. Yu, L. Yang, L. Zhu, X. Jian, Z. Wang, L. Jiang, J. Power Sources 191 (2009) 495–500.
[15] M.C. Li, C.L. Zeng, S.Z. Luo, J.N. Shen, H.C. Lin, C.N. Cao, Electrochim. Acta 48 (2003) 1735–1741.
[16] H. Wang, M.A. Sweikart, J.A. Turner, J. Power Sources 115 (2003) 243–251.
[17] S.J. Lee, C.H. Huang, J.J. Lai, Y.P. Chen, J. Power Sources 131 (2004) 162–168.
[18] H. Wang, J.A. Turner, J. Power Sources 128 (2004) 193–200.
[19] H. Wang, M.P. Brady, K.L. More, H.M. Mayer III, J.A. Turner, J. Power Sources 138 (2004) 79–85.
[20] H. Wang, M.P. Brady, G. Teeter, J.A. Turner, J. Power Sources 138 (2004) 86–93.
[21] J. Jayaraj, Y.C. Kim, K.B. Kim, H.K. Seok, E. Fleury, Sci. Technol. Adv. Mater 6 (2005) 282–289.
[22] Y. Wang, D.O. Northwood, Int. J. Hydrogen Energy 32 (2007) 895–902.
[23] D.P. Davies, P.L. Adcock, M. Turpin, S.J. Rowen, J. Appl. Electrochem. 30 (2000) 101–105.
[24] Y.J. Ren, C.L. Zeng, J. Power Sources 171 (2007) 778–782.
[25] W.-Y. Ho, H.-J. Pan, C.-L. Chang, D.-Y. Wang, J.J. Hwang, Surf. Coat. Technol. 202 (2007) 1297–1301.
[26] K.H. Cho, W.G. Lee, S.B. Lee, H. Jang, J. Power Sources 178 (2008) 671–676.
[27] Ch.-Y. Chung, Sh.-K. Chen, P-J. Chiu, M.-Hs. Chang, T.-Ts. Hung, Ts.-H. Ko, J. Power Sources 176 (2008) 276–281.
[28] V.V. Nikam, R.G. Reddy, S.R. Collins, P.C. Williams, G.H. Schiroky, G.W. Henrich, Electrochim. Acta 53 (2007) 2743–2750.
[29] M. Kumagai, S.-T. Myung, S. Kuwata, R. Asaishi, H. Yashiro, Electrochim. Acta 53 (2008) 4205–4212.
[30] S.J. Lee, C.H. Huang, Y.P. Chen, J. Mater. Process. Technol. 140 (2003) 688–693.
[31] Y. Wang, D.O. Northwood, J. Power Sources 163 (2006) 500–508.
[32] Y. Wang, D.O. Northwood, J. Power Sources 165 (2007) 293–298.
[33] H. Wang, J.A. Turner, J. Power Sources 170 (2007) 387–394.
[34] Y. Hung, K.M. El-Khatib, H. Tawfik, J. Appl. Electrochem. 35 (2005) 445–447.
[35] Y. Hung, K.M. El-Khatib, H. Tawfik, J. Power Sources 163 (2006) 509–513.
[36] S.-H. Wang, J. Peng, W.-B. Lui, J.-S. Zhang, J. Power Sources 162 (2006) 486–491.
[37] S. Kitta, H. Uchida, M. Watanabe, Electrichim. Acta 53 (2007) 2025–2033.
[38] Z.E. Dunbar, R.I. Masel, J. Power Sources 182 (2008) 76–82.
[39] L. Stockert, F. Hunkeler, H. Bohni, Corrosion 41 (1985) 676–677.
[40] I.-S. Lee, E.E. Stansbury, S.J. Pawel, Corrosion 45 (1989) 134–136.
[41] T. Kinumoto, M. Inaba, Y. Nakayama, K. Ogata, R. Umebayashi, A. Tasaka, Y. Iriyama, T. Abe, Z. Ogumi, J. Power Sources 58 (2006) 1222–1228.
[42] A. Pozio, R.F. Silva, M. De Francesco, L. De Giorgi, Electrochim. Acta 48 (2003) 1543–1549.
[43] D. Pletcher, I. Whyte, F.C. Walsh, J.P. Millington, J. Appl. Electrochem. 21 (1991) 659–666.
[44] ASTM Designation: G15-04 – Standard Terminology Relating to Corrosion and Corrosion Testing, 2004.
[45] A.A. Hermes, M.S. Morad, Corros. Sci. 50 (2008) 2710–2717.
[46] ASTM Designation: G61-86R03: Standard Test Method for Conducting Cyclic Potentiodynamic Polarization Measurements for Localized Corrosion Susceptibility of Iron-, Nickel-, or Cobalt-Based Alloys, 1997.
[47] T. Bellezze, G. Roventi, R. Fratesi, Electrochim. Acta 49 (2004) 3005–3014.
[48] G. Palumbo, P.J. King, K.T. Aust, Corrosion 43 (1987) 37–45.
[49] Y.M. Zeng, J.L. Luo, P.R. Norton, Electrochim. Acta 49 (2004) 703–714.
[50] P.T. Jakobsen, E. Maahan, Corros. Sci. 43 (2001) 1693–1709.
[51] S.N. Simison, S.R. de Sanchez, D.J. Schiffrin, Corrosion 45 (1989) 967–970.
[52] V. Čihal, R. Štefec, Electrochim. Acta 46 (2001) 3867–3877.
[53] B.E. Wilde, in: R.W. Staehle, B.F. Brown, J. Kruger, A. Agarwal (Eds.), Localized Corrosion, NACE, Houston, TX, 1974, p. 342.
[54] L.J. Korb, D.L. Olson, ASM Handbook, vol. 13: Corrosion, American Society for Metals, Metals Park, OH, 1992, pp. 236–244.
[55] M. Pourbaix, Corrosion 26 (1970) 431.
[56] Y.M. Liou, S.Y. Chiu, C.L. Lee, H.C. Shih, J. Appl. Electrochem. 29 (1999) 1377–1381.
[57] G.S. Frankel, M. Rohwerder, in: M. Stratmann, G.S. Frankel (Eds.), Encyclopedia of Electrochemistry, vol. 4: Corrosion and Oxide Films, Wiley VCH, Weinheim (D), 2003, pp. 697–700.